ISSN (Print) 1226-1750
ISSN (Online) 2233-6656
Journal of Magnetics 20(4), 387-393 (2015) http://dx.doi.org/10.4283/JMAG.2015.20.4.387

An Asymmetric Rotor Design of Interior Permanent Magnet Synchronous Motor for Improving Torque Performance

Myung-Hwan Yoon[1], Doo-Young Kim[1], Sung-Il Kim[2], and Jung-Pyo Hong[1]*

[1]*Department of Automotive Engineering, Hanyang University, Seoul 04763, Korea*
[2]*Motor R&D Group, Digital Appliances, Samsung Electronics, Suwon 16674, Korea*

(Received 4 August 2015, Received in final form 28 November 2015, Accepted 1 December 2015)

Torque ripple is necessarily generated in interior permanent magnet synchronous motors (IPMSMs) due to the non-sinusoidal distribution of flux density in the air gap and the magnetic reluctance by stator slots. This paper deals with an asymmetric rotor shape to reduce torque ripple which can make sinusoidal flux density distribution in the air gap. Meanwhile the average torque is relatively increased by the asymmetric rotor. Response surface method (RSM) is applied to find the optimum position of the permanent magnets for the IMPSM with improved torque performance. Consequently, an asymmetric structure is the result of RSM and the structure has disadvantage of a mechanical stiffness. Finally, the performance of suggested shape is verified by finite element analysis and structural analysis is conducted for the mechanical stiffness.

Keywords : average torque, torque ripple, flux distribution, permanent magnet position, rotor core saturation, response surface methodology

1. Introduction

Interior permanent magnet synchronous motors (IPMSMs) have many merits such as high torque density, high efficiency and a wide speed range of operation which can be achieved by flux weakening control. Therefore, IPMSMs are widely used in automotive application where space and energy savings are critical. These days wound field rotor synchronous motors and spoke type motors are studied, because the price of rare-earth material is not stable. However, these motors have lower efficiency and lower torque density compared to the motors using rare-earth material. The total resultant instantaneous torque of a synchronous permanent magnet motor has two components: an average torque and a pulsating torque which causes torque ripple. There are three reasons for torque pulsation. First one is the field harmonic torque due to the non-ideal spatial distribution of flux density in the air-gap, in other words, non-sinusoidal flux density in IPMSMs. The second source of torque ripple is the cogging torque caused by virtue of the reluctance torque which exists between permanent magnet and stator slot. The third one is the reluctance torque generated by unequal permeances of direct and quadrature axis. This torque is produced by the self-inductance variations of the phase windings as magnetic circuits of direct and quadrature axis are unbalanced. Researches of reducing torque ripple have been carried out for a long time and can be classified into two categories which are the points of view of design and control [1-15]. In this paper, a method to reduce torque ripple is suggested by the point of view of motor design. Conventional methods for the reduction of torque ripple such as the pole-arc to pole pitch ratio, slot/pole number combinations, skew [3, 4], and rotor shaping [7, 8] are studied. Modifying rotor shape can make a sinusoidal flux density distribution in the air gap which results in reduction of the noise and vibration [7, 8] and stator iron loss, and also improve efficiency. The most important point is that torque ripple can be reduced by modifying the rotor shape, but an average torque can be also decreased. However, this paper suggests the method of reducing torque ripple and increasing the average torque at the same time by adjusting saturation of rotor core. The distribution of flux density in air gap can be sinusoidal by controlling the saturation of rotor core with the consideration of armature reaction. Response surface methodology (RSM) is applied to find out the optimum location of permanent magnet. Consequently, the characteristics of

*Corresponding author: Tel: +82-2-2220-0455
Fax: +82-2-2220-4465, e-mail: hongjp@hanyang.ac.kr

final model are verified by finite element analysis and compared with original model. Structural analysis is conducted for checking a mechanical stiffness.

2. Fundamental Theory

Armature reaction is one of the factors which cause the non-sinusoidal distribution of flux density in air gap. Fig. 1(a) shows the flux density distribution due to the rotor field alone, while Fig. 1(b) shows the armature magneto-motive force (MMF) distribution due to the induced current of stator. And the resultant flux distribution is shown in Fig. 1(c). As shown in Fig. 1, the armature reaction causes a decrease of the resultant air gap flux density in a half of the pole and increase in the other half. Therefore, the flux density which is enhanced by the armature reaction should be reduced in order to make sinusoidal flux density distribution in the air gap. According to the ohm's law for magnetic circuits, the air gap flux density is expressed by

$$B = \frac{F}{SR_t}, \tag{1}$$

where B is the flux density, F is the resultant MMF, S is the cross section area, and R_t is the total reluctance of magnetic circuit, which is given by

$$R_t = R_g + R_c + R_p, \tag{2}$$

where R_g is the reluctance of air gap, R_c is the reluctance of iron core and R_p is the reluctance of the permanent magnet. Reluctance is given by

$$R = \frac{1}{\mu S}, \tag{3}$$

where l is the length of magnet and μ is a permeability.

Flux density can be reduced by increase of reluctance as MMF is constant. Applying salient pole shoes is an effective method to increase the air gap reluctance of particular parts, which reduces the torque ripple and cogging torque. According to equation (2), the total reluctance has three components and the reluctance of iron core is small due to the great value of permeability. In this paper, the part of rotor core where the flux density is increased is designed to be saturated. As a result, the permeability of the part decreases which results in increase of the total reluctance. Afterwards, sinusoidal distribution of flux density can be obtained and torque ripple can be reduced.

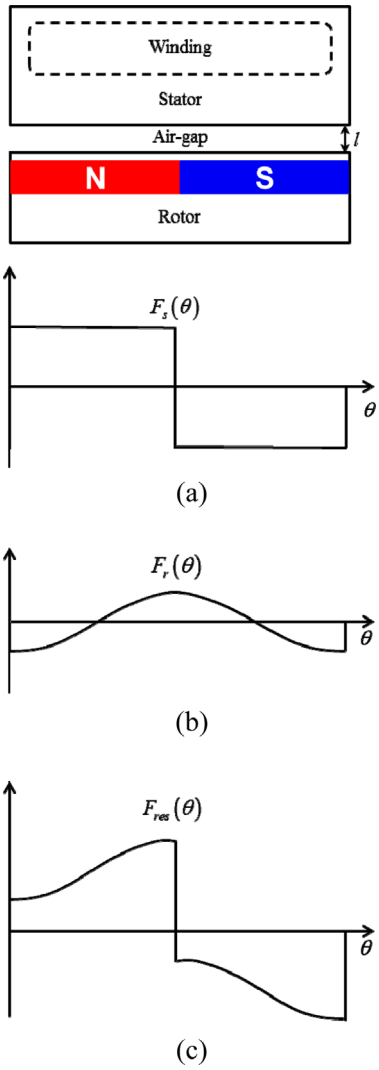

Fig. 1. (Color online) (a) Flux density distribution due to the rotor field (b) due to armature MMF (c) Resultant flux density distribution.

3. Optimization of Rotor Configuration

3.1. Original Model

The original model is shown in Fig. 2. 1/3 model of 6 pole/36 slot motor is used for the analysis and the optimization. Dimensions of the motor are shown in Table 1.

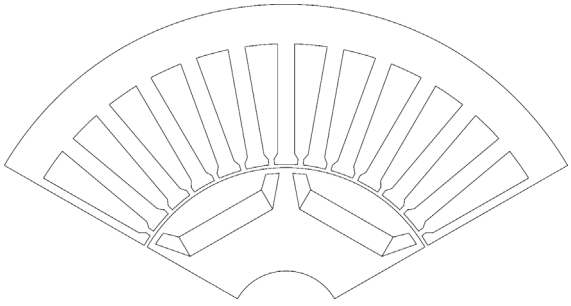

Fig. 2. 6 pole/ 36 slot motor.

Table 1. Dimensions of original model.

	Value	Unit
Pole / slot number	6 / 36	-
Stack length	90	mm
Stator outer diameter	116	mm
Rotor & stator material	35PN230	

3.2. Optimum Design

RSM explains the relationships among several design variables. Values or range satisfying torque performances are calculated by RSM. The objectives are to minimize torque ripple and maximize average torque. Design variables are three directions for the position of permanent magnet which are shown in Fig. 3.

Three variables are x axial displacement, y axial displacement and rotating angle on the basis of center of the permanent magnet. Minitab, which is a statistical tool, is applied to conduct RSM.

The formula is expressed as follows

$$f_{net} = w_1 \cdot f_{ripple}(x, y, \alpha) - w_2 \cdot f_{avg}(x, y, \alpha) \,. \quad (4)$$

Optimization is conducted by minimization of f_{net} which is the sum of torque ripple and average torque with negative value.

where, w_1 and w_2 are weighting factors, $f_{ripple}(x, y, \alpha)$ and $f_{avg}(x, y, \alpha)$ are the values of torque ripple and average torque respectively according to the position of permanent magnet with variables of x, y and α.

The moveable area of permanent magnet is restricted to the minimum thickness for ribs of the motor and the range of variables is shown in Table 2. In other words, size of permanent magnet, pole arc and the thickness of rib are fixed as shown in Fig. 3. The optimum solution and the tendency of objective function can be achieved as 15 models are analyzed which is provided by Minitab as shown in Fig. 4, Fig 5, and Fig 6. Central composite design is applied to decide 15 models for the RSM. The result of optimization is presented in Table 3.

As shown in Table 3, the optimized values for x, y and

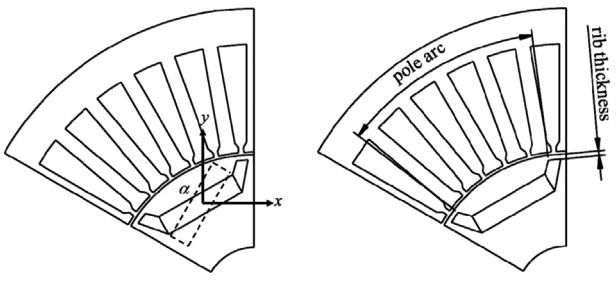

Fig. 3. Variables and constraints of RSM.

Table 2. Range of variables.

Variables	Range	Unit
x	−1~0.8	mm
y	0~0.6	mm
α	0~12	degree

Table 3. Result of RSM.

Variables	Range	Optimized value	Unit
x	−1~0.8	−0.1	mm
y	0~0.6	0.6	mm
α	0~12	12	degree

α are −0.1 mm, 0.6 mm, and 12° respectively. Optimum solution is also shown in Fig. 6. Minitab which is used for the RSM in this paper, calculates an individual desir-

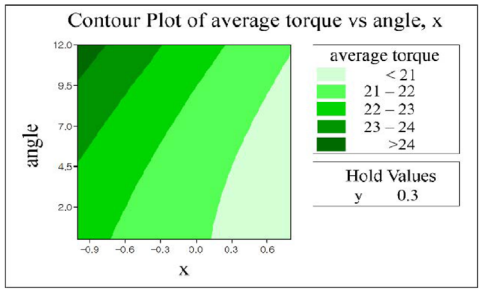

(a)

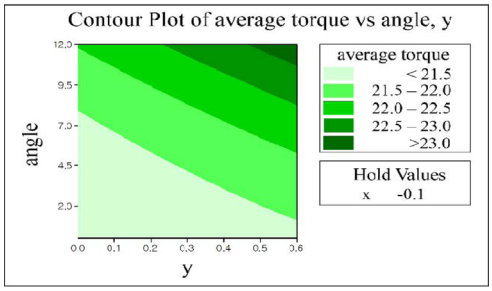

(b)

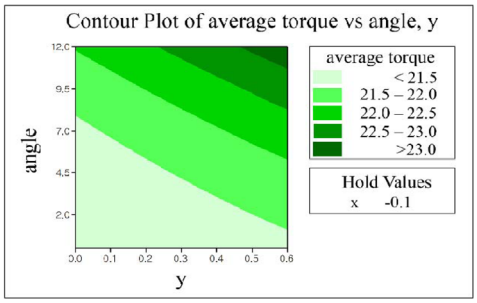

(c)

Fig. 4. (Color online) Tendency of average torque with changing factors (a) x and α (b) y and α (c) x and y.

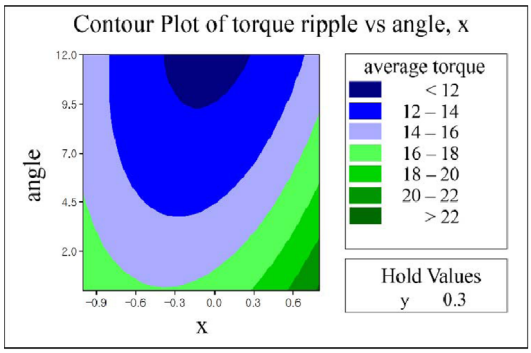

(a)

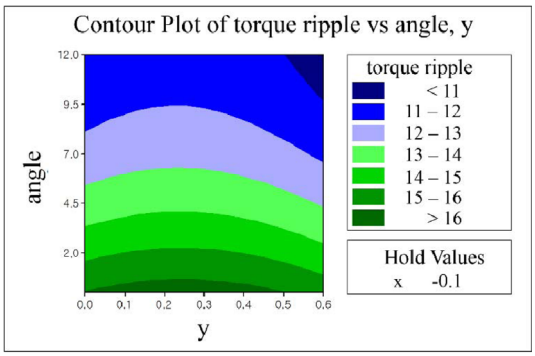

(b)

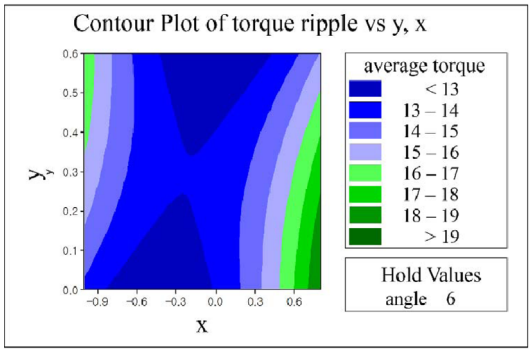

(c)

Fig. 5. (Color online) Tendency of torque ripple according to factors (a) x and α (b) y and α (c) x and y.

ability for each response and they are combined to provide a measure of the composite desirability of the multi-response system. Individual and composite desirability assess how well a combination of input variables satisfies the goal defined for the responses. Desirability has a range of zero to one. One represents the ideal case and zero indicates that one or more responses are outside their acceptable limits. In other words, as desirability is close to 1, favorable results can be obtained. The letter d and the letter y on the left column mean the individual desirability and the response value for each response respectively.

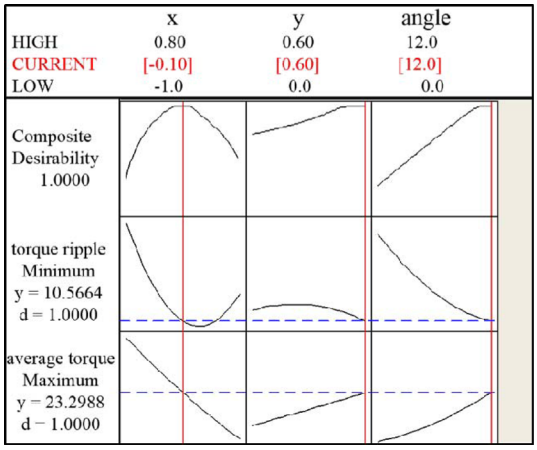

Fig. 6. (Color online) Optimum solution.

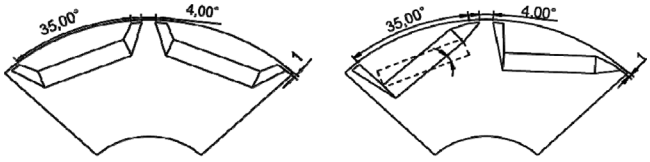

(a) (b)

Fig. 7. Rotor shape of (a) original model (b) optimized model.

Core between the air gap and the permanent magnet is thin on the right side and thick on the left side for the optimized model as shown in Fig. 7. The position of permanent magnet for the optimized model is changed from the original model. The area of the optimized model is thinner than that of the original model, which makes it easier to be saturated.

4. Characteristics Comparison

4.1. Current Angle 0°

Both original model and optimized model are analyzed under the same current condition which is described in Table 4. Current angle 0° model is analyzed to verify this method. EMF, which is an in-house code for finite element analysis, is used to analyze the performances of this two models, such as flux density distribution, flux linkage of each phase, and saturation of motors, etc. Comparison of average torque and torque ripple are shown in Fig. 8 and Table 5. As shown in Table 5, the torque ripple decreases from 16.81% to 9.91%. Meanwhile, the average torque

Table 4. Analysis condition.

List	Value
Driving type	Sinewave
Current magnitude [A_{rms}]	140

Table 5. Result comparison.

List	Max. Torque [Nm]	Min. Torque [Nm]	Avg. Torque [Nm]	Torque Ripple [%]
Original model	22.71	19.21	20.83	16.81
Optimized model	25.31	22.73	23.31	9.91

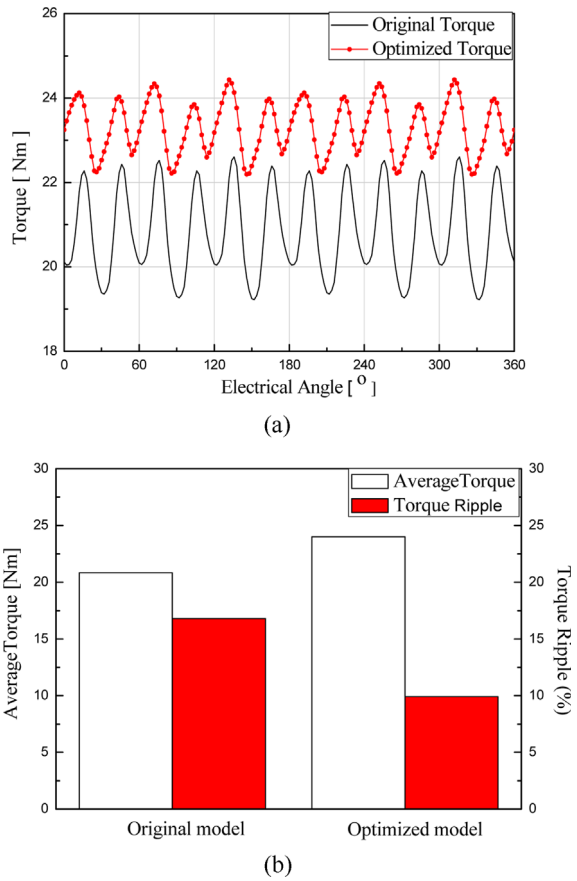

Fig. 8. (Color online) Comparison of torque ripple and average torque.

increases from 20.83 Nm to 23.31 Nm. The proposed method is verified by these results with increased average torque and decreased torque ripple.

Figure 9 and Fig. 10 show the flux density distribution in rotor core and air gap, respectively. As expected, the thin part of core between permanent magnet and air gap in Fig. 9 is saturated compared to the thicker part of core. The total harmonic distortion (THD) of original model and optimized model are 25.63% and 26.77%. Although both torque ripple and average torque are improved by this proposed method, THD is similar. Figure 11 shows the line to line induced voltage and the THD of two motors at 1000RPM, respectively. The induced voltage for the optimized model is $32.58V_{rms}$ which is reduced from that of original model, $32.72V_{rms}$.

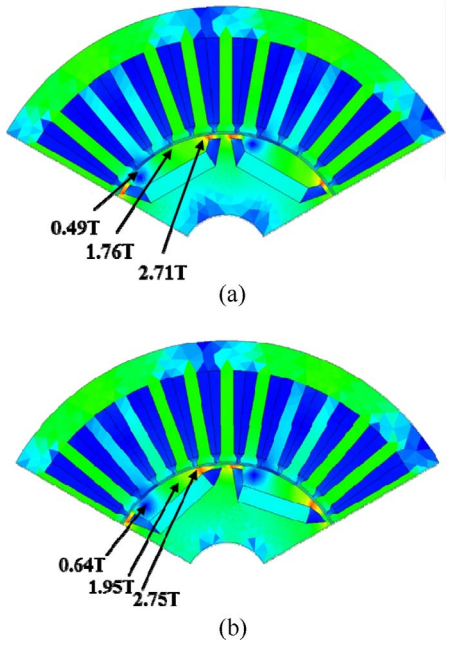

Fig. 9. (Color online) Flux density distribution in rotor core for (a) original model and (b) optimized model.

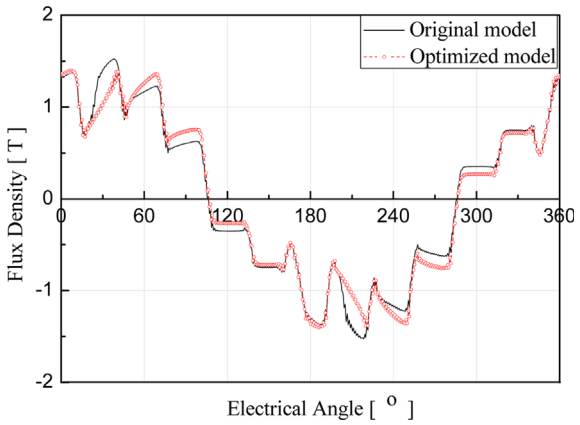

Fig. 10. (Color online) Flux density distribution in air gap for original model and optimized model.

4.2. Characteristics According to Current Angle

Since this method is proved to be effective as current angle is 0°, however IPMSMs are generally driven by current angle which is greater than 0°. The validity of this method under other current angle conditions are necessary to be verified as well. Accordingly, the two models are

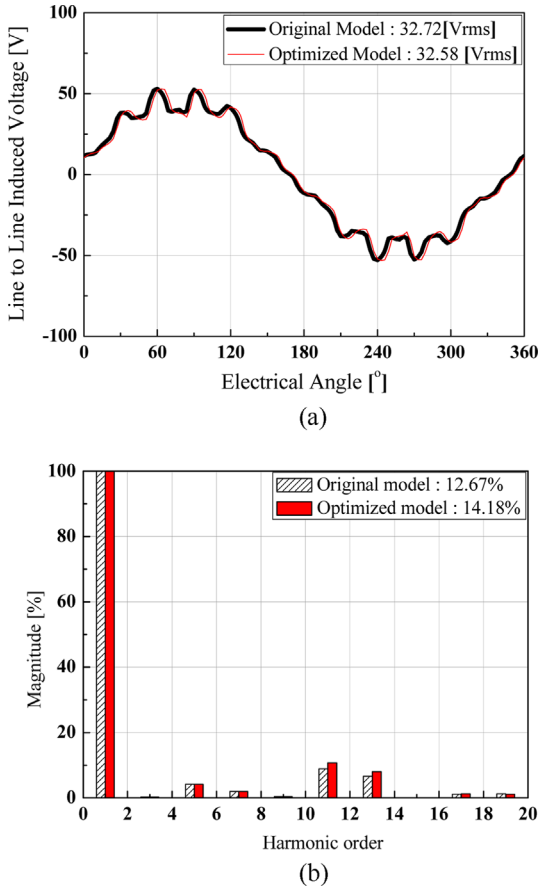

Fig. 11. (Color online) (a) Line to line induced voltage (@1000RPM) (b) Total harmonic distortion.

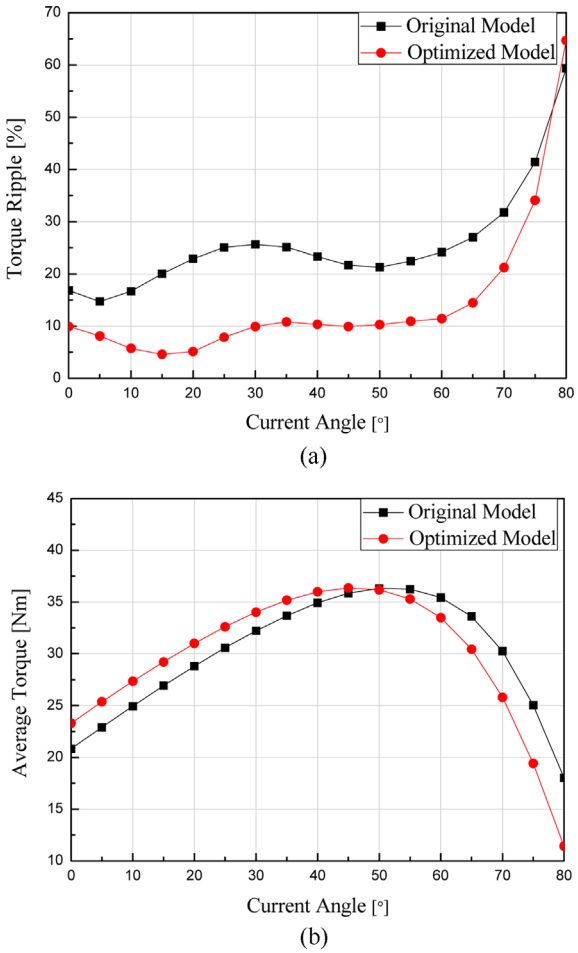

Fig. 12. (Color online) (a) Torque ripple according to current angle (b) average torque according to current angle.

computed by the current angle in the range from 0° to 80° with the same current magnitude, which is 140 A_{rms}. The results are shown in Fig. 12. As the current angle is between 0° and 75°, the torque ripple decreases while the average torque increases as the angle is between 0° and 50°. In other words, this method is effective for this model in case the current angle is in the range from 0° to 50°. The appropriate current angle can be obtained by the suggested method.

5. Structural Analysis and Comparison

In this paper, a structural analysis is conducted for examining mechanical stiffness of two models. ANSYS, which is a finite element analysis tool for the structural analysis, is used for this paper. Boundary conditions are shown in Fig. 13 and speed of analysis is 4500RPM. As a result, the maximum stress of original model is 13.5 MPa,

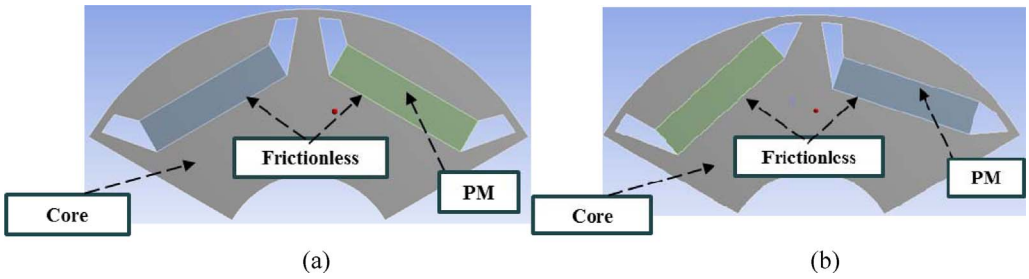

Fig. 13. (Color online) Boundary conditions for (a) original model (b) optimized model.

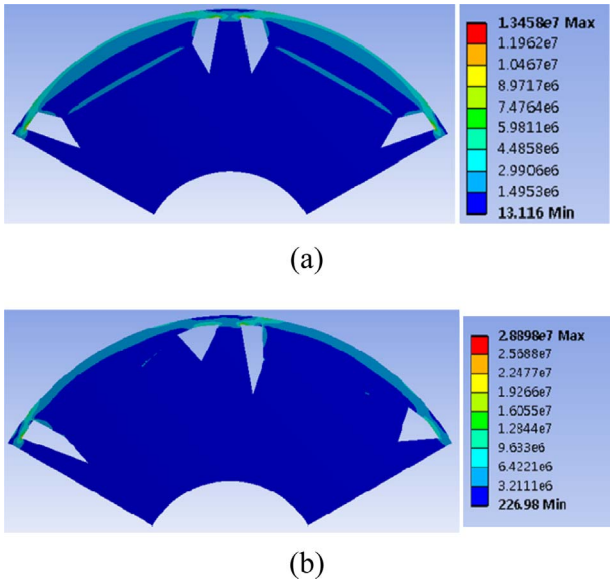

Fig. 14. (Color online) Result of structural analysis (a) original model (b) optimized model.

but that of optimized model is 28.9 MPa. The stress for optimized model is approximately twice greater than the value for original model. Therefore, structural analysis is necessary for designing asymmetric model.

6. Conclusions

In this paper, optimum design of rotor is conducted to improve the torque performance of IPMSMs which is verified by finite element analysis with an asymmetric structures of permanent magnet and barrier. Increased average torque and decreased torque ripple can be obtained by applying the suggested method. However, the structure of the optimum model has a disadvantage of a mechanical stiffness. The asymmetric structure model, which is suggested in this paper, can be applied to various field as the trade-off between the torque performance and the mechanical stiffness is considered.

Acknowledgements

This research was supported by the MSIP (Ministry of Science, ICT and Future Planning), Korea, under the C-ITRC (Convergence Information Technology Research Center) (IITP-2015-H8601-15-1005) supervised by the IITP (Institute for Information & communications Technology Promotion).

References

[1] S. A. Evans, IEEE. ICEM, 1 (2010).
[2] L. Fang, S. I. Kim, S. O. Kwon, and J. P. Hong, IEEE. Trans. Magn. **46**, 2183 (2010).
[3] S. M. Hwang, J. B. Eom, Y. H. Jung, and D. W. Lee, IEEE. Trans. Magn. **37**, 2806 (2001).
[4] M. Gulec and M. Aydin, IET Electr. Power Appl. **8**, 189 (2014).
[5] D. Iles-Klumpner, U.S. Patent No. 7, 230 (2007).
[6] S. I. Kim, J. Y. Lee, Y. K. Kim, and J. P. Hong, IEEE. Trans. Magn. **41**, 1796 (2005).
[7] S. I. Kim, Y. K. Kim, G. H. Lee, and J. P. Hong, IEEE. Trans. Magn. **48**, 843 (2012).
[8] K. Wang, Z. Q. Zhu, G. Ombach, and W. Chlebosz, IEEE. ICEM, 397 (2012).
[9] S. I. Kim, G. H. Lee, J. J. Lee, and J. P. Hong, IJAT **11**, 277 (2010).
[10] G. H. Lee, W. C. Choi, S. I. Kim, S. O. Kwon, and J. P. Hong, IJAT **11**, 291 (2011).
[11] H. Shang, L. Zhao, and T. Wang, IEEE. ICISCE, 1001 (2015).
[12] P. Zheng, W. Ke, Z. Song, Q. Zhao, and J. Bai, Electrical Machines and Systems IEEE. ICEMS, 1 (2011).
[13] K. W. Jeon, T. Y. Lee, Y. J. Kim, and S. Y. Jung, IET. CEM 2014, 1 (2014).
[14] Y. U. Park, J. U. Cho, D. H. Chung, J. Y. So, and D. K Kim, IEEE. ICEM, 1139 (2013).
[15] D. Wnag, X. Wang, and S. Y. Jung, IEEE. Trans. Magn. **49**, 2295 (2013).